

Visual Optimality and Stability Analysis of 3DCT Scan Positions

Artem Amirkhanov, Christoph Heinzl, Michael Reiter, and M. Eduard Gröller

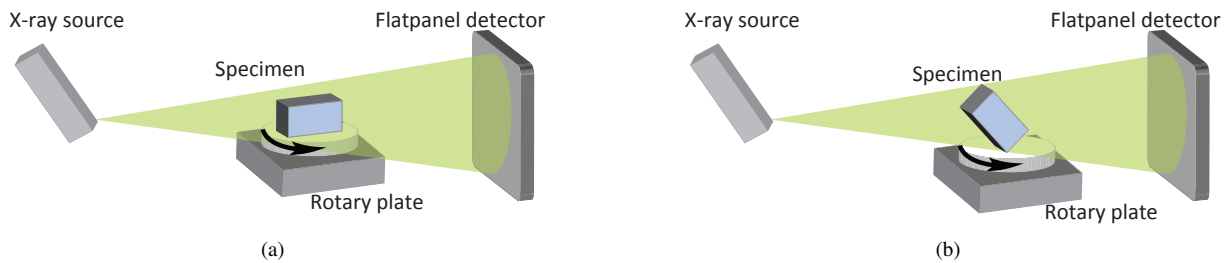


Fig. 1. Geometry of the 3DCT circular cone-beam scanning system. Example of a bad placement (a) and a good placement (b) of a specimen on a rotary plate.

Abstract—Industrial cone-beam X-Ray computed tomography (CT) systems often face problems due to artifacts caused by a bad placement of the specimen on the rotary plate. This paper presents a visual-analysis tool for CT systems, which provides a simulation-based preview and estimates artifacts and deviations of a specimen's placement using the corresponding 3D geometrical surface model as input. The presented tool identifies potentially good or bad placements of a specimen and regions of a specimen, which cause the major portion of artefacts. The tool can be used for a preliminary analysis of the specimen before CT scanning, in order to determine the optimal way of placing the object. The analysis includes: penetration lengths, placement stability and an investigation in Radon space. Novel visualization techniques are applied to the simulation data. A stability widget is presented for determining the placement parameters' robustness. The performance and the comparison of results provided by the tool compared with real world data is demonstrated using two specimens.

1 INTRODUCTION

Three-dimensional computed tomography (3DCT) is a powerful technique for producing a digital 3D volumetric dataset of an object from 2D X-ray penetration images. The main advantage of 3DCT is its ability to capture both the interior and the exterior structure of a specimen including a detailed material characterization in one single scan. Having been used in medical diagnostics for a long time, 3DCT is increasingly employed in industry as a method for nondestructive testing and quality control. A new and challenging application in the field of industrial computed tomography is metrology, which has to fulfill the demands of today's standards in industrial quality control. In comparison to methods of conventional metrology, 3DCT is the only method, which facilitates dimensional measurements of the internal structure and of inaccessible parts of a component.

Figure 1 shows the typical scheme of an industrial CT system. The test specimen is placed on the rotary plate, which is located between an X-ray radiation source and a flat panel detector. The cone-beam radiation produced by the X-ray source is penetrating the specimen and generates a grayscale attenuation image on the detector. In order to obtain all the necessary projections of an object for a full scan, the specimen is rotated stepwise on the rotary table. A 360 degree rotation is typically used for a full reconstruction of the 3D dataset. The rotation corresponds to a circular source trajectory of the cone-beam CT. This circular cone-beam (CB) scanning scheme is commonly used in

industrial X-ray 3DCT and is considered in this paper. Usually 720 projections of the specimen are taken. This requires typical scan times of about 30 minutes [5]. Filtered back projection is then applied to reconstruct a volume dataset from the set of projections. The Feldkamp algorithm (FDK) [3] is the reconstruction method, which is widely used for 3D industrial cone-beam CT scanning. Industrial CT has its own peculiarities and problems compared to medical CT. In engineering, multi-material components are very common, which are manufactured of weak absorbing plastics carrier structures in the neighborhood of strongly absorbing metal components. Scanning these parts generates severe artifacts in the datasets. Additionally the material and density have high dynamic ranges, which complicate the tuning of 3DCT devices. Medical CT systems are optimized on a well defined application area with well-known materials such as blood, tissue or bone. As a young application field, industrial 3DCT does not yet have established protocols or generally applicable metrology standards that can be relied upon. One of the most critical issues in the area of metrology using industrial 3DCT is the problem of artifacts. Artifacts are artificial structures in the reconstructed dataset, which do not correspond to structures of the measured specimen. In the area of metrology artifacts may seriously affect or even prevent reliable measurements [5]. The appearance of artifacts results in measurement deviations from the reference dataset.

Some of the most common artifact types are noise induced streaks, beam hardening, partial volume effects, aliasing, and scattered radiation [6]. For polychromatic radiation as used in 3DCT the correlation between attenuation and penetration length is nonlinear. The polychromatic spectrum of an X-ray beam is hardened as it traverses through matter. This means that higher energies of the spectrum are passing through the matter, while lower energy photons are absorbed. What is remaining is a modified spectrum containing mainly the higher energy portions. Thus, thicker objects reduce radiation by a smaller amount per unit length compared to thinner objects [5]. This effect is called beam-hardening. Beam-hardening causes two types of artifacts: cupping artifacts and the appearance of bright or dark bands or streaks between dense objects in the image [1]. In cone-beam CT the char-

• Artem Amirkhanov and M. Eduard Gröller are with the Institute of Computer Graphics and Algorithms, Vienna University of Technology, Austria. E-mail: {artem, groeller}@cg.tuwien.ac.at.

• Christoph Heinzl and Michael Reiter are with the Upper Austrian University of Applied Sciences, Wels Campus, Austria. E-mail: {christoph.heinzl, michael.reiter}@fh-wels.at.

Manuscript received 31 March 2010; accepted 1 August 2010; posted online 24 October 2010; mailed on 16 October 2010.

For information on obtaining reprints of this article, please send email to: tvcg@computer.org.

acteristics and magnitude of an artifact are mainly determined by the specimen's geometry, its position and orientation in the cone beam, the measurement parameters and the specimen's material combination.

In this paper we focus on artifacts depending on the specimen placement on the rotary plate. Finding an optimal specimen placement is crucial for the technicians. In many cases picking the appropriate specimen placement reduces the amount of artifacts and significantly improves measurement accuracy. An example of a good and a bad positioning of a specimen is given in Figure 1. Placement (a) has high penetration lengths and top and bottom faces which will produce heavy artifacts. Placement (b) has shorter penetration lengths and good face orientations. Currently, the optimal placement of a specimen is based on the knowledge and experience of the technicians. The adoption of this knowledge on specimens with a complex geometry is subjective and quite difficult even for the domain specialists. Scanning a specimen several times in order to find the optimal placement is not an alternative due to the long overall machine occupation times and high costs. Another issue is the complexity of comparing the 3DCT results.

In this situation, technicians require a visual analysis tool to determine the optimal specimen placement. The proposed tool provides a simulation-based preview and it is able to estimate artifacts and deviations for every placement.

After consultations with industrial 3DCT domain experts we identified three criteria for what is defined as a good specimen placement. The requirements for a good specimen placement are formulated as follows:

- short cone-beam penetration lengths
- no surface data lost during scanning
- the penetration lengths and lost surface data parameters are stable within a certain range of reliability (usually about 5 degrees)

In the following paragraphs we consider these conditions in greater detail.

The penetration length of a ray is defined as the distance, which the ray passes inside the specimen. A high penetration length of an X-ray is prone to cause beam-hardening artifacts and may consequently reduce the accuracy of measurements. Therefore, the penetration length is a very important parameter, which we want to minimize in order to decrease deviations and improve measurement accuracy.

When cone-beam scans are used, for some of the planar faces of the specimen an exact reconstruction is not possible due to the incompleteness of the acquisition geometry [22] [25]. For this reason these planar faces will appear blurred in the resulting reconstructed volume. Corresponding to Tuy-Smith [18] the sufficiency condition for a full reconstruction is the following: if on every plane, that intersects the object there exists at least one point of the X-ray source trajectory, then one can fully reconstruct the object. For an accurate reconstruction of an arbitrary plane, it should intersect the circular trajectory of the source. Applying this criterion to the faces of the specimen we get the following: a face can be accurately reconstructed if its plane has an intersection with the circular trajectory of the source. The Tuy-Smith data sufficiency condition [18] helps to identify blurred faces. These faces are nearly perpendicular to the rotation axis and have a big height offset from the X-ray source's position. An example of bad faces is given in Figure 2. As we can see from this example, we can get rid of the bad faces by choosing a proper placement of a specimen. Minimizing the total surface area of faces, which do not satisfy the Tuy-Smith data sufficiency condition, will result in better scan results.

The above mentioned parameters should remain stable within a certain range of placement variability, as the technicians are able to setup the orientation of a specimen only with certain accuracy. Usually it lies within a range of 1-5 degrees. The stability of a placement determines how fast a parameter (e.g., maximum penetration length) changes when the orientation of the placement is modified. Small modifications in the orientation of a specimen may cause strong changes in the considered parameter and therefore in the scanning result. The less the placement's parameter changes with a modification of the orientation,

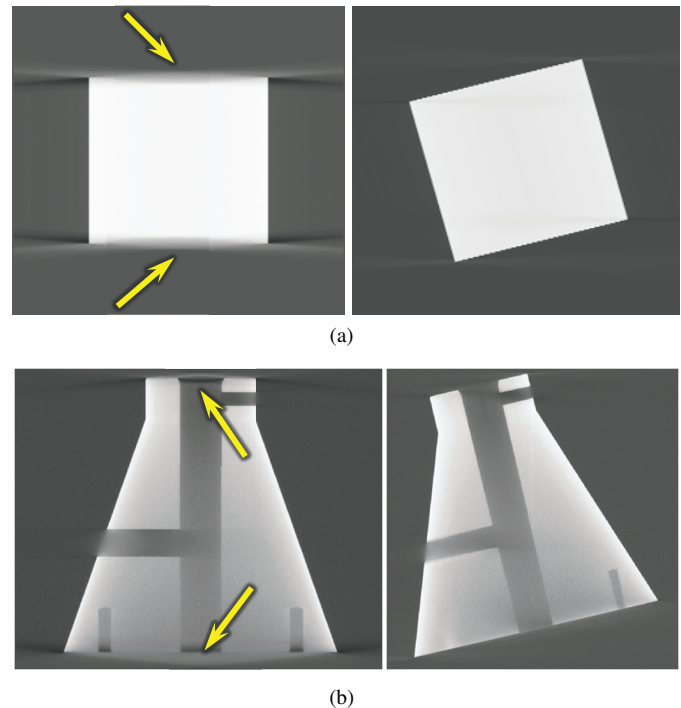


Fig. 2. Example of bad faces for the cube specimen (a) and for the TP03 specimen (b). Artifacts are marked with yellow arrows. The placements to the left are worse than the placements to the right.

the more stable the placement is. If the parameters of the placement are changing considerably, then the orientation is considered to be inappropriate because of its instability. Thus, the stability of a placement is another decisive factor for choosing an optimal placement.

In quality control of new products manufacturers test representative samples of each production charge for compliance with quality requirements and the presence of defects. CAD geometrical models are used as reference. In other cases (e.g., reverse-engineering) a geometrical surface model may be obtained through CT or optical scans. The geometrical surface model of the specimen can therefore be used as input data for the simulation and evaluation of an optimal placement.

In this paper we present a visual analysis tool that determines optimal placements of a specimen on a rotary plate using the following criteria:

- **Short cone-beam penetration lengths:** based on a ray casting simulation (section 3)
- **No surface data lost during scanning:** based on the Radon-space analysis (section 4)
- **the penetration lengths and lost surface data parameters are stable within a certain range of reliability:** using the stability widget (section 5)

An overview of the workflow of the visual analysis tool is presented in Figure 3. Concerning placement, we consider only the orientation of a specimen on the rotary plate. The orientation is defined by two degrees of freedom, as the third degree of freedom corresponds to the rotation of the specimen on the rotary plate. The position of a specimen on the rotary plate is not considered because it would make the computational complexity of the simulation too high. Moreover, the position of the specimen has a small influence on the outcome of the simulation and insignificantly changes the optimal orientation value. The tool allows further visualization, exploration and visual analysis of the obtained data (section 6). The main contributions of this paper are the application of easy to understand visualization methods on

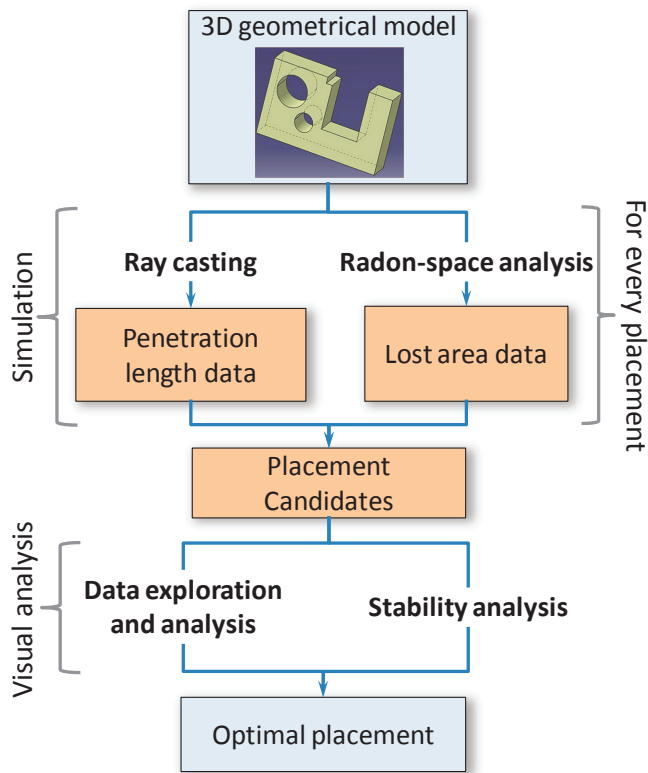


Fig. 3. Workflow of determining an optimal specimen placement.

the penetration-length data and the Radon-space analysis data; visual analysis of the parameter variability using a stability widget; ray visualizations and Radon-space analysis.

2 RELATED WORK

Multi-image views are used by Malik et al. [9] for a visual exploration and comparison of a dataset series generated by scanning a specimen with different parameters on an industrial CT device. Common CT simulation approaches as Monte-Carlo simulations [7] [10], hybrid approaches [4] [19] and discrete simulations [16] of CT are used to predict the results of real measurements by computing the interaction of virtual X-rays with matter. Such a prediction helps the technician in measurement technology to minimize artifacts by using optimal measurement parameters. Monte Carlo and related simulation methods are more complex and computationally expensive. We focus on penetration lengths and do not address a detailed simulation of the X-ray attenuation and interaction with matter.

Camera control and viewpoint selection for the polygonal and volumetric data are well investigated research areas. Vázquez et al. [23] worked on the problem of defining a ‘good’ view. They use viewpoint entropy to evaluate the quality of a viewpoint. Bordoloi and Shen [2] use viewpoint entropy in volume rendering to determine a minimal set of representative views for a given scene. The importance of single voxels and the similarity between viewpoints are taken into account for their viewpoint-selection process. A feature-driven approach to select a good viewpoint is proposed by Takahashi et al. [20]. They propose to decompose an entire volume into a set of feature components, and then find a globally optimal viewpoint by taking a compromise between locally optimal viewpoints. Viola et al. [24] introduced another automatic viewpoint-selection approach for features in a volume dataset. The focus feature is defined by the user and their system automatically determines the most expressive view on this feature. Mühlner et al. [11] presented an approach for viewpoint selection in medical surface visualizations. They describe a viewpoint-selection technique guided by weighted parameters like size of unoccluded surface, im-

portance of occluding objects, preferred region and viewpoint stability. Viewpoint stability is used to avoid viewpoints where the object of interest is occluded by small changes of the camera.

There are various approaches implemented to select a region of interest (ROI) in the inspected object. When a ROI is specified for volume data this region is also called volume of interest (VOI). Tory and Swindells [21] presented ExoVis for detail and context direct volume rendering. They define a VOI by specifying a box within the volume. Different transfer functions can be used for the picked region. Owada et al. [13] presented a technique to specify a ROI within unsegmented volume data. The user specifies the 2D contour of the interesting structure and the system performs a constrained segmentation based on statistical region merging.

The main purpose of a viewpoint selection is to provide an expressive view of the data. We focus on finding the specimen placement with optimal parameters for the 3DCT scanning. The placement stability is defined by the behavior of these parameters when the orientation of the specimen is changed.

Missing Radon space data during CB scanning is a well studied phenomenon. Zhu et al. [25] analyze the CB projections in Radon space and apply implicit interpolation/extrapolation to the missing data in order to reduce beam-hardening artefacts. We are not aware of any existing related work, which applies a Radon space analysis of triangles using the Tuy-Smith data-sufficiency condition.

3 PENETRATION-LENGTH ANALYSIS

Concerning penetration-length analysis there are two important factors which determine the overall optimality of a placement: how long are penetrations and how many rays have high penetration lengths. In this respect, we use two parameters to characterize a placement: the maximum penetration length and the average penetration length. The maximum penetration length is the longest distance that an X-ray beam has to travel inside the specimen. The average penetration length is the average distance, which the radiation has to go through the specimen in order to reach the detector.

We employ ray casting to calculate the penetration lengths. Basically we could calculate penetration lengths through rasterization, i.e., surface rendering on the GPU. We have decided to use ray casting, even if it is more costly. The main reason is the flexibility and extendibility, which ray casting offers. This concerns the calculation of additional parameters that the simulation might require (e.g., the scattered radiation contribution to the results). Another possible approach is a purely analytical computation of maximum and average penetration lengths. The decisive disadvantage of this approach is the high complexity of the calculations. For instance, in order to calculate the average penetration length of one projection, we need to calculate the volume from the surface mesh and divide it by the surface area of this mesh projected on the detector plane. Computing the maximum penetration length is also a nontrivial task when using a purely analytical approach. On the other hand, ray casting provides a good approximation to the average and maximum penetration lengths.

The ray-casting geometry in our approach reflects the real-world scanning-device setup. The source of the X-ray radiation corresponds to the ray origin. We cast a ray for every X-ray cell on the flat-panel detector and the result is stored in a single pixel. We substitute the specimen with its 3D geometrical model represented by a list of triangles. We further use data about the setup of the scanning device to configure the ray casting geometry.

The simulation is computed for a discrete set of possible placements. Every placement is determined by its orientation. The position of the specimen on the rotary plate is fixed. The orientation is determined by two Euler angles α and β . We obtain the successive placement in a set by changing one of the Euler angles by a certain step-angle. The user-defined number of angle samples and angle range determine the step-angle. For every placement in a set we perform ray casting and calculate the penetration lengths.

The data that we get from the ray casting is represented in three layers: rays, projections, and placements. A placement consists of a sequence of projections. The projections of a placement are obtained

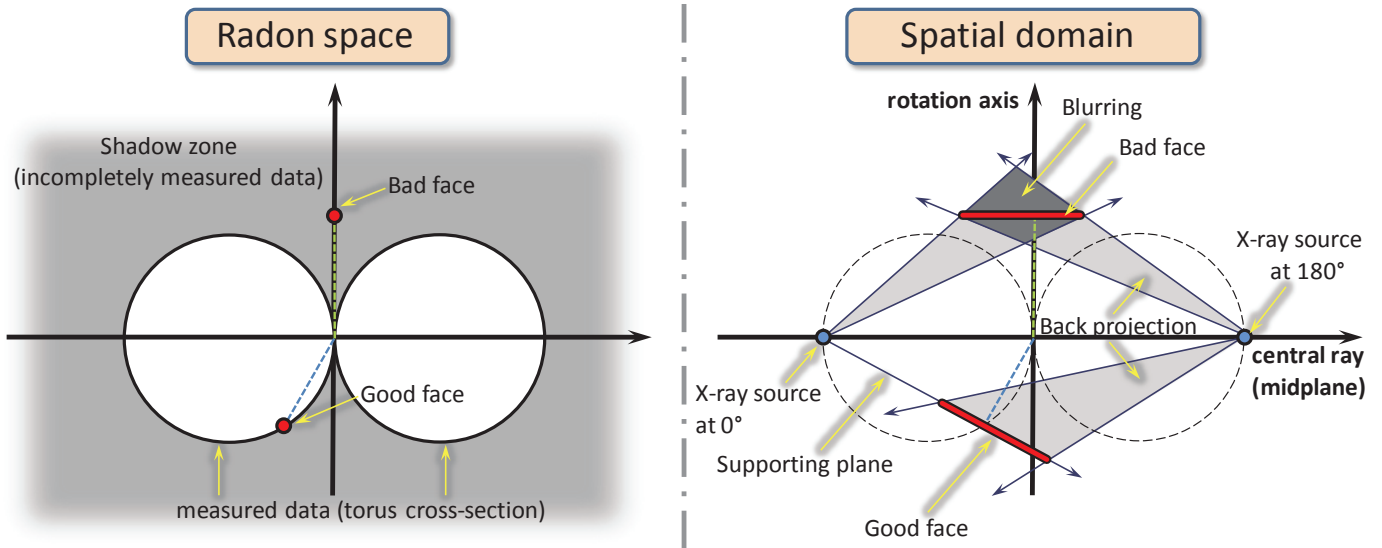


Fig. 4. Cross-section through Radon space (left) and the spatial domain (right). The two white circles in the left image correspond to a cross-section through the torus. The rest is the shadow zone. Examples of good and bad faces are given.

rotating the specimen around a vertical rotation axis. Every projection in its turn is obtained by casting a set of rays.

The penetration length is calculated for every ray of a placement. We calculate the penetration length of a ray as the sum of distances, which the ray passes inside the specimen. The average penetration length of a projection is calculated as average of the penetration lengths from the corresponding rays. Finally, the average penetration length of a placement is calculated as average of the penetration lengths from the corresponding projections. In addition for every projection and placement the maximum penetration lengths are determined. The maximum penetration length of a projection is the maximum from all the corresponding rays. Finally the maximum penetration length of a placement is the maximum from all corresponding projections.

In order to speed up the ray-casting step we implemented parallelized CPU and GPU (CUDA coded) versions. We use a k -dimensional tree (kd -tree) as a space-partitioning data structure. A stack-based algorithm for traversing the kd -tree is employed.

4 RADON-SPACE ANALYSIS

Cone-beam CT devices using the FDK reconstruction algorithm suffer from a specific kind of artifact: inaccurate reconstruction of some planar faces of the object, which are not in the midplane. The midplane is the plane that contains all the points of the source trajectory. For the circular cone-beam scanning this is a plane perpendicular to the rotation axis. These artifacts lead to a blurring of the reconstructed volume and, therefore, reduce the measurement accuracy. The presence of the artifacts strongly depends on the specimen placement. We want to find the placement, which has no bad faces or which has the smallest surface area of such faces.

4.1 Background and Theory

Reconstruction from projections as done in 3DCT is closely related to the Radon transform. Let a 3D function f be defined on the domain D . The continuous 3D Radon transform maps a function in \mathcal{R}^3 into the set of its plane integrals in \mathcal{R}^3 . The Radon transform \check{f} of function f , which is specified by a vector \vec{n} , is given by:

$$\check{f}(\vec{n}) = \int_{\vec{r} \in P(\vec{n})} f(\vec{r}) d\vec{r} \quad (1)$$

where P is a 2D plane, with a normal vector collinear to \vec{n} and a displacement $|\vec{n}|$ from the origin (i.e., the point on the rotation axis located on the same height as the X-ray source). The Radon transform

maps every plane in the spatial domain to a point in Radon space. The mapping is done in a way that the position vector of this point has the same direction as the plane's normal. And the length of the position vector is equal to the distance from the plane to the origin. This mapping was first studied in detail by Radon [15] in 1917. Radon showed that if \check{f} is continuous, then there exists a unique and analytic inverse transform. The 3DCT scanning samples the Radon transform \check{f} of the object. Reconstruction algorithms as the filtered back projection approximate the inversion.

With circular cone-beam (CB) scanning the cone-beam X-ray source is rotated around the object. The situation where a specimen is rotated on a rotary plate is considered as a circular scan. The circular CB trajectory only partially satisfies the Tuy-Smith sufficiency condition. For some faces of the scanned object, there are no corresponding points of the circular CB source trajectory, which lie on the supporting planes of these faces. This means that it is impossible to completely measure all information about these planes of the scanned object with the Radon transform. Only at the midplane (plane of the source trajectory) an exact reconstruction is possible. For one CB projection, the surface of a sphere is acquired in Radon space. The diameter of the sphere is equal to the distance from the X-ray source to the rotation center. As the rotary plate turns, the sphere rotates as well. With a full scan, a torus is measured in the Radon space (see Figure 4). The higher the number of projections, the better the Radon transform is sampled inside the torus. The part of information in Radon space, which is not inside the torus, forms a shadow zone. If the supporting plane of the face lies in the shadow zone, then Tuy-Smith's sufficiency condition does not hold. If the supporting plane of the face is inside the torus in Radon space then Tuy-Smith's sufficiency condition is true for this face. All faces of the specimen that are perpendicular to the rotation axis (except those in the midplane) are in the shadow zone. Furthermore, all the faces whose supporting planes do not intersect the circular trajectory of the source are in the shadow zone as well. Faces of the specimen that lie in a shadow zone will produce back-projection artifacts. These artifacts appear in the direction of the back projection and blur object faces on the scanned projection images. An example of a bad face and a good face is given in Figure 4.

4.2 Radon-space Analysis

The goal of the Radon-space analysis is to minimize the total surface area of object triangles, whose supporting planes are outside the torus of measured data in Radon space. Therefore we calculate for every placement the Radon-space representation of all triangles of the spec-

imen surface. Every triangle is represented as a point in Radon space. The position vector of this point has the same direction as the triangle's normal and the length equal to the distance from the supporting plane of the triangle to the origin in the spatial domain. We check whether the point in Radon space is inside the torus of measured data or not. As a result we calculate the total surface area of triangles whose Radon information is not sufficiently captured during the scanning. The placement with the minimal lost surface area is considered to be the optimal one. We use the percentage of the lost surface area as another parameter in our visual analysis system. Triangles causing back-projection artifacts are color coded in red (see section 6.4).

The Radon-space investigation determines the areas which cause back-projection artifacts. As the method requires only angles between triangle planes and the rotation axis, we need to do calculations just once for a placement. We do not need to process the entire sequence of projections (as we have to do in the ray-casting simulation).

5 PLACEMENT-STABILITY ANALYSIS

After the penetration-length analysis and the Radon-space analysis, the stability of the determined optimal placements is evaluated. Typically technicians are capable of placing the specimen on the rotary plate with a placement error between 1-5 degrees. This imposes the following limitation for the optimal placement: the results of the penetration-length analysis and the Radon-space analysis should remain stable within this range. In this respect, we require a tool for the visual analysis of the robustness of the placement's parameters in a considered range. The tool should allow a distinction between improvement and deterioration of the parameters along certain directions. Another desirable feature of the tool is the ability to show in which direction parameters vary the most. For this purpose we use a custom stability widget as visualization technique (see Figure 5). We pick a parameter and a placement in order to see how the parameter changes when we change the orientation of the specimen. Deviations for the selected parameter (e.g., maximum penetration length) are shown on the stability widget. The central cell on the widget represents the specimen's current placement. Neighboring cells correspond to the placements obtained by stepwise changing either of the two Euler angles. The horizontal axis of the color-coded map corresponds to the α Euler angle and the vertical axis corresponds to the β Euler angle. The deviation of the parameter from the central placement is color-coded. Green colors correspond to better positions and red to worse positions. The maximum deviations, which are obtained by changing only one of the Euler angles keeping the other Euler angle fixed, are coded as gray values on so called stability arrows. Stability arrows are applied for extracting information about the stability of a placement in a certain direction. For example, dark gray corresponds to a rather instable behavior on that axis and white corresponds to stable conditions.

Using the stability widget in the example of Figure 5 the β direction is more stable than the α direction. If we change the orientation of the specimen along the β axis in positive or negative direction, the parameter value will gradually improve. The worst case would be changing the α angle in positive direction. Considering the fact that the parameter changes only gradually in all directions, this placement is robust and stable.

The main purpose of the stability widget is to visually explore the robustness of the placements, and the visual analysis and immediate recognition of patterns. However, a fully automated stability analysis could be implemented. For example, it is possible to automatically reject the placements with great instability. In this work we focus on the visual exploration and analysis of placements where an automatic categorization is not easily possible.

6 DATA VISUALIZATION, EXPLORATION AND VISUAL ANALYSIS.

6.1 Visualization of Placement Parameters.

The parameters of every placement in a set are represented using color-coded maps and 3D plots. The 3D plot representation is used for a better visual representation of the data. The color-coded map representation is used for navigation and user interactions. Every pixel of

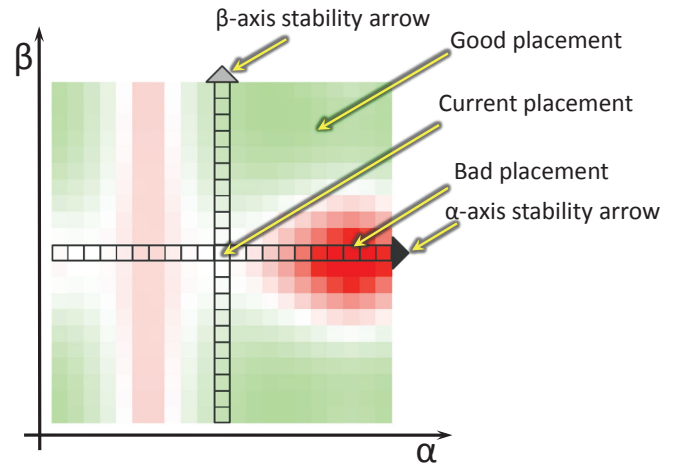


Fig. 5. Widget representing the stability of the specimen's placement.

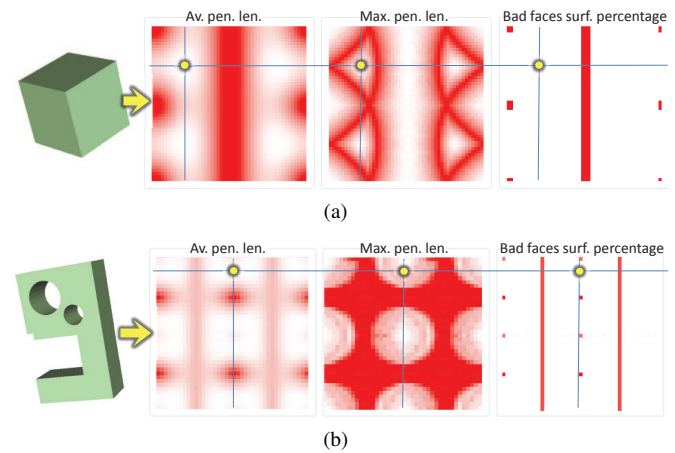


Fig. 6. Linked views used for the comparative visualization of the cube specimen (a) and of the TP09 specimen (b). The good placement is highlighted.

the color-coded map or vertex of the 3D plot is colored according to the value of a placement parameter. The horizontal axis of the color-coded map corresponds to the α Euler angle and the vertical axis corresponds to the β Euler angle. The user gets numerical labels of the parameters of a placement and its orientation by clicking in the color-coded map. The 3D view of the specimen is automatically updated so that the specimen is placed using the orientation of the picked placement. In addition the user can select a certain percentage of the placements with the best parameter values on the color-map using a slider. The discarded placements will be displayed in black.

6.2 Comparative Visualisation of Placement Parameters.

To visualize the different parameters we use linked views in a side-by-side visualization (see Figure 6). There is one map for every parameter. When the user is picking a placement in one map the others are updated as well, so that the picked placement is highlighted in all maps.

6.3 Feature Selection

In many cases technicians are interested in accurate scan results for certain critical features or areas of interest in the specimen. In this case they need a tool to select critical features (e.g., drill holes) and to calculate placements, which are appropriate for these features only. We allow the user to select certain features of the specimen. We do the

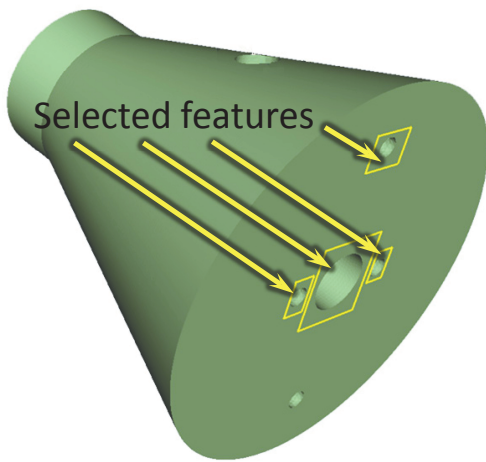


Fig. 7. Selected features represented in the 3D view of the specimen's geometrical model.

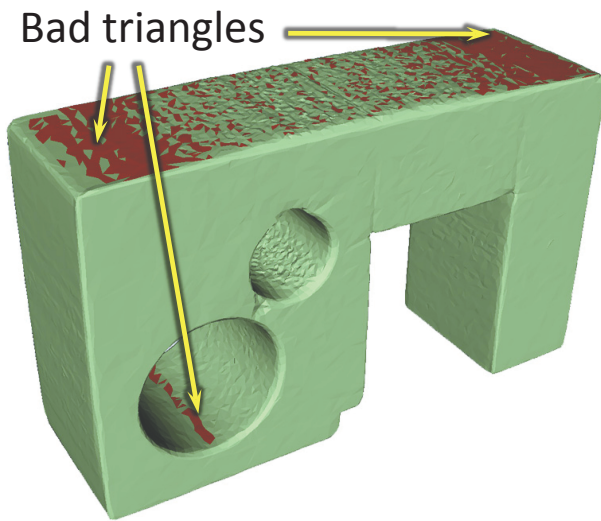


Fig. 8. Color coding the results of the Radon space investigation on the surface model of test part TP09. Triangles shown in red are outside the torus of the measured Radon data.

selection by specifying a set of axis-aligned bounding boxes (AABB) around the features of interest (see Figure 7). The user can add new boxes, select boxes by picking them in a list and delete them from the list. The extent of a box is changed using sliders. After the set of the bounding boxes is specified, all parameters are evaluated just for these boxes. Only rays which intersect one of the specified bounding boxes are processed during the ray-casting process. Only triangles which are fully inside one of the bounding boxes are used in the Radon space investigation.

6.4 Color-coding Bad Areas

In order to visualize the results of the Radon-space investigation we color code the triangles, which are outside of the torus of measured data in the Radon space. Color coding of bad surface areas on the 3D geometrical model of a regular aluminium test part (Kasperl [8]) is shown in Figure 8. This surface model was extracted by reengineering the corresponding 3DCT dataset. We can clearly see the artifacts between the two drill-holes, the vertical stripes on the sides and the distorted top of the specimen.

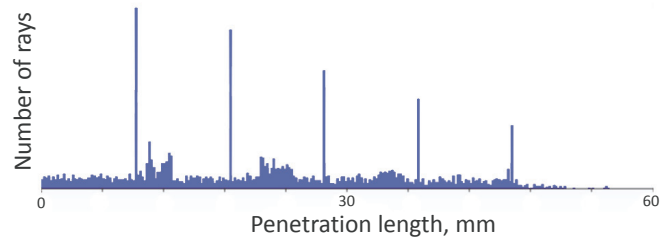


Fig. 9. Example of penetration length histogram.

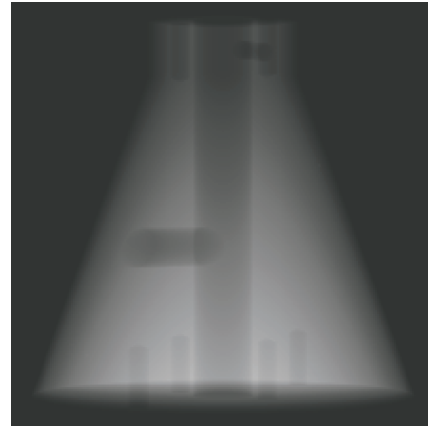


Fig. 10. Visualizing the penetration lengths of a single projection in grayscale.

6.5 Penetration-Length Histograms

Another helpful component is building histograms of the rays' penetration-length distributions (see Figure 9). To build a histogram the user specifies the placement he is interested in and picks the desired parameter. Such histograms are useful when we need to see how many rays have penetration lengths in a critical range. Histograms also allow to see how uniformly the rays are distributed for the picked parameter. For example, if only a few of the rays have high penetration lengths or most of the penetration lengths are in some narrow range, then the placement can be considered as being good. On the other hand, if most of the rays have high penetration lengths or the range of the penetration lengths is large then the placement should not be used in 3DCT scanning. In addition, the user can build a histogram for a single projection of placement.

6.6 Visualization of Ray Subsets

Often the penetration-length histograms do not show all the information required to make a proper decision. In this case a visualization of the penetration lengths of single projection is helpful. We show the direct output of the ray-casting simulation using grayscale images (see Figure 10). The greater the penetrations of rays are, the brighter are the corresponding pixels.

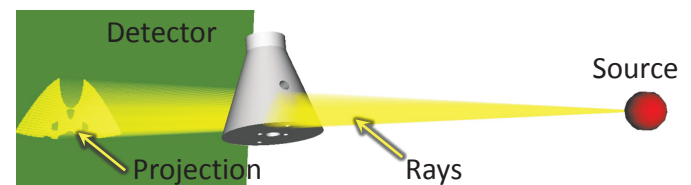


Fig. 11. Visualizing rays with penetration length in a specified range. Rays are drawn as semi-transparent yellow lines. The green plane represents the detector. The red sphere is the X-ray source.

In order to determine problematic areas we visualize rays within a certain range of penetration lengths. The user specifies the projection and the penetration lengths he is interested in. The rays with corresponding penetration lengths are visualized using semi-transparent lines. The corresponding detector points are highlighted with point sprites (see Figure 11). This visualization represents geometrical information about areas of the specimen with high penetration lengths and shows the corresponding regions on the detector or resulting image.

7 IMPLEMENTATION AND PERFORMANCE

The prototype application was implemented in Visual C++. The interactive 3D view was implemented using VTK [17]. The GPU ray-casting implementation was coded using CUDA [12].

7.1 Parallelization

The set of placements of the specimen that we need to process is known in advance. Calculations for rays are also independent from each other. Thus, there are two possible ways of parallelization: parallelization on the level of the projections and parallelization on the level of the rays.

In the CPU implementation the screen is split into tiles. Every tile is processed by a separate thread. The assignment of the threads to the processor's cores is done by the operating system. The GPU architecture on the other hand is highly parallel and can execute thousands of threads. Every ray is processed in a single thread.

When the resolution of a projection image is lower than the maximum number of threads that the GPU can handle, not all of the GPU capabilities are used. In the GPU implementation we therefore process several projections in one pass. Several projections are treated as a single image. For instance, the set of n projections with resolution $x \times x$ will be rendered as an image with a resolution of $x \times x \times n$ pixels. Rays corresponding to different projections have origin and direction vectors according to the projection's rotation angle. This strategy is called batch rendering as we process a batch of the projections in one call of the kernel function. Batch rendering uses most of the GPU capabilities, because the number of threads processed with a single call of the kernel function increases.

7.2 Performance

Ray casting is a crucial part in the entire system performance. So, in this section we will concentrate only on the performance of the ray-casting step. The most important parameters for the GPU performance are: the resolution and the complexity of the specimen's geometrical model. Table 1 shows a performance comparison of the CPU and GPU implementations. The GPU performance depends on the resolution, number of triangles in the model and the batch size. The GPU implementation is 1.1 to 6 times faster than the CPU implementation. The GPU implementation shows good results on small geometrical models and high resolutions. On the other hand, when the geometrical model is big, threads are computationally complex and have many conditional branches in the kd -tree traversing algorithm. The GPU implementation does not provide any significant improvement compared to the CPU implementation.

Our implementation is relatively slow compared to existing GPU ray-tracers (e.g., work by Popov et al. [14]). There are two main factors that influence the performance of our implementation. First, in our implementation we cannot use early ray termination as we need to find every ray-specimen intersection. Second, we have to do data streaming from the GPU memory back to the CPU memory in order to store the simulation results.

8 RESULTS

8.1 Evaluation

The general workflow of using the system is as follows. First, the user selects the features of interest on the geometrical model. Then the system calculates the penetration-lengths data and does the Radon-space investigation for the set of placements. Based on the obtained

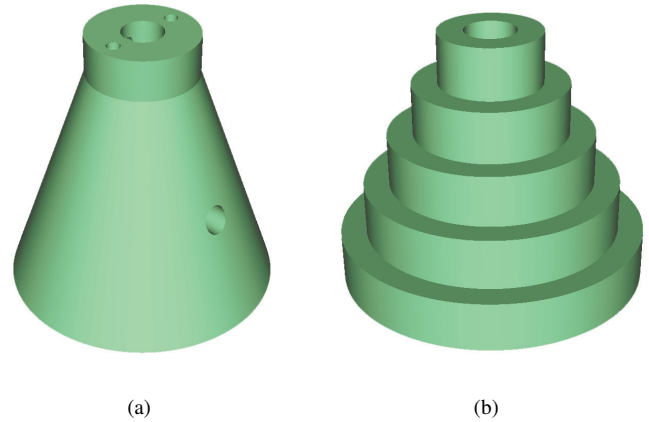


Fig. 12. The specimens used for the evaluation: TP03 (a), a cone with attached cylinder, a large central drill hole and several minor drill holes; a TP07 step-cylinder (b) with a central drill hole.

data, the system proposes a set of candidates for the optimal placement. Afterwards the user determines the optimal placement using the visual-analysis functionality provided by the tool. The user should pick a placement with the minimal maximum-penetration length and the shortest possible average penetration length. There should be only small surface areas affected by the Tuy-Smith data-insufficiency condition in Radon-space. Furthermore the above mentioned criteria should remain stable within the possible positioning accuracy of 1-5 degrees. This means that the picked placement should be stable. Finally, the user applies the determined placement for the specimen positioning on the rotary plate.

For the evaluation of the presented method a set of scans with different specimen placements was measured. A fixed set of measurement features for every placement was evaluated using the commercial CT metrology software 'Calypso' from Carl Zeiss IMT Corporation Germany. Calypso is a standard tool in the area of coordinate measuring machines and multidimensional metrology. For every measurement feature (e.g., length, diameter, roundness, evenness etc.) this tool interpolates a predefined number of points along the corresponding geometry primitive (e.g., line, circle, cylinder, plane, etc.) in order to extract the dimension of interest. Instead of extracting the exact dimensions themselves, we calculate the sigma value for every feature measurement as this represents the underlying data quality. Sigma is thereby the standard deviation of the measurement points along the geometry of the primitive. A smaller sigma indicates a better scan and measurement quality. Using our tool we provide the average and the maximum penetration lengths and the percentage of the lost surface area for all of the selected features. To evaluate the simulation results, we compare the sigma values with results provided by our tool. We use two specimens for the evaluation. These specimens are shown in Figure 12. For the TP03 specimen the scans were done for placements with α equal to 0, 10, 45, 70 and 90 degrees. As we can see from the comparison of the results, there is a significant correspondence between the percentage of the lost surface area and the accuracy of linear distance measurements. The penetration-length simulation predicts good placements for the drill-hole radius measurements. Tables 2 and 3 show the sigma values of the features in the CT measurements and penetration lengths of these features for all α values of the TP03 specimen. The optimal placement for every feature is given in bold font. We can see that the placement proposed according to the average penetration length is coincident with the optimal placement for features A, B, C, D and E. The average penetration length predicts optimal placements for 5 features out of 9. The maximum penetration length correctly proposes optimal placements for the features A, E, F, H and placement with sigma within the maximum error range (0,01 mm) for the features B, C and I. The maximum penetration length pre-

Table 1. Comparison of the CPU and GPU ray-casting time in seconds on the various triangulated models. CPU: Intel Core i7, 920 @ 2.67 GHz. GPU: NVIDIA GeForce GTX 260.

Number of triangles	Resolution of projections	Number of projections	CPU time, s		GPU time, s		
			Batch size				
			10	30	50		
12	256×256	1000	16.864	3.963	3.042	2.761	
310	256×256	1000	18.127	7.411	6.271	6.037	
25880	256×256	1000	27.612	25.038	23.749	23.400	
25880	1024×1024	100	39.562	16.676	-	-	
200000	256×256	1000	78.281	43.446	42.229	41.871	

Table 2. Sigma values of the features in the CT measurements for the TP03 specimen.

Feature	Sigma value, mm				
	0	10	45	70	90
A	0,040	0,041	0,079	0,110	0,134
B	0,015	0,013	0,023	0,167	0,102
C	0,014	0,013	0,020	0,030	0,132
D	0,019	0,006	0,013	0,013	0,017
E	0,032	0,037	0,063	0,086	0,137
F	0,084	0,038	0,068	0,080	0,021
G	0,172	0,064	0,010	0,023	0,022
H	0,080	0,044	0,025	0,023	0,041
I	0,066	0,038	0,026	0,033	0,215

Table 3. Average and maximum penetration lengths of the TP03 specimen's features.

Feature	Average penetr. len., mm					Maximum penetr. len., mm				
	0	10	45	70	90	0	10	45	70	90
A	53	53	54	60	60	95	97	102	119	119
B	25	25	29	46	40	38	40	73	119	105
C	25	25	29	46	40	38	40	73	119	105
D	24	24	36	52	54	37	39	77	119	115
E	50	50	58	65	62	74	74	102	117	108
F	67	58	35	34	41	95	96	77	76	72
G	66	70	66	60	40	95	95	102	110	72
H	76	75	58	57	52	95	97	93	92	100
I	76	75	58	57	53	95	97	94	92	100

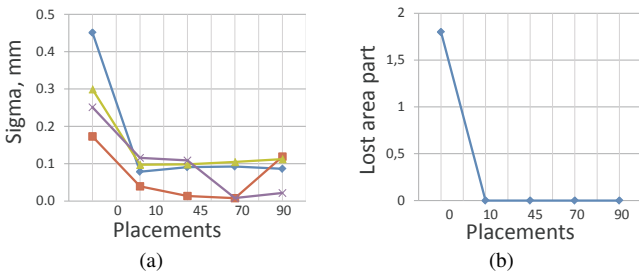


Fig. 13. The plots of the sigma values of the linear distance features (a) and the percentage of the lost surface area (b) for the TP03 specimen.

dicts 7 features out of 9. The G feature is not predicted by any of the parameters. The maximum penetration length correctly predicts more placements than the average penetration length. However, the D feature is correctly predicted only by the average penetration length.

The plots of the sigma values of the linear distance features and the percentage of the lost surface area for the TP03 specimen are given in Figure 13. We see that the placement with an α value of 0 degree has the highest lost surface percentage and the highest sigma values. We also compared the bad surface areas obtained by the Radon-space investigation with the reconstruction images (see Figure 14). We can see that there is a strong correspondence between the results of the Radon-space investigation and the real world data.

As second specimen, to evaluate the proposed method with, the test part TP07 is used. This specimen represents a step-cylinder with a central drill hole. Different α values of the specimen have been analyzed. The placements corresponding to α equal to 0, 10, 20, 30, 40, 50, 60, 70, 80 and 90 degrees were used. Diameters and heights of every cylinder step were measured. We use the percentage of the lost surface area to evaluate the heights (linear distance measurements), and penetration lengths to evaluate the drill-hole radius measurements. Tables

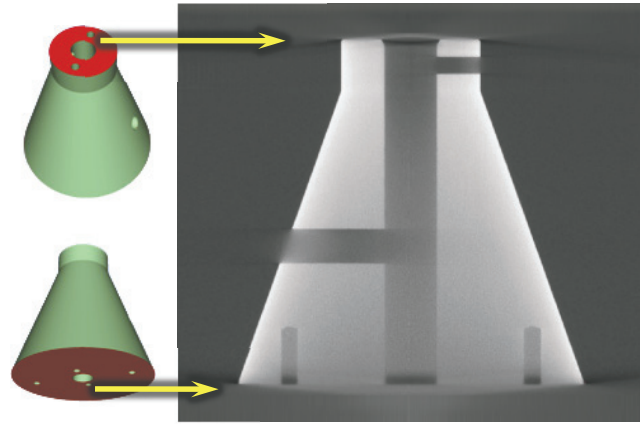


Fig. 14. Comparison of the bad surface areas obtained by the Radon-space investigation with the reconstruction images for the TP03 test specimen. Surface areas causing back-projection artifacts are outside of the torus of measured Radon data and shown in red.

4 and 5 show sigma values of the features in the CT measurements, and penetration lengths of these features for every placement of the TP07 specimen. The placements proposed by the average penetration length are coincident with the optimal placement for features O-C2, O-C3, I-C1 and I-C2. The proposed placement is nearly optimal for the feature I-C4. The average penetration length predicts 5 features out of 7. The maximum penetration length proposes optimal placements exactly for the features O-C2, O-C3, O-C4, I-C1 and I-C2. The proposed placement is nearly optimal for the feature I-C3. The maximum penetration length thus predicts 6 features out of 7. The same as in the previous case, the maximum penetration length correctly predicts more placements than the average penetration length. However, the I-C4 feature is better predicted by the average penetration length.

Table 4. Sigma values of the features in the CT measurements for the TP07 specimen. The features are named as follows: 'O' stands for the outer diameter, 'I' stands for the inner diameter, 'C' stands for the step-cylinders from top to bottom.

Feature	Sigma value, mm									
	0	10	20	30	40	50	60	70	80	90
O-C2	0,002	0,002	0,004	0,006	0,007	0,009	0,007	0,009	0,012	0,008
O-C3	0,002	0,003	0,005	0,006	0,006	0,008	0,007	0,008	0,008	0,008
O-C4	0,002	0,005	0,004	0,006	0,006	0,007	0,006	0,006	0,005	0,013
I-C1	0,004	0,004	0,005	0,005	0,006	0,011	0,006	0,017	0,018	0,019
I-C2	0,005	0,005	0,006	0,006	0,007	-	0,011	0,015	0,017	0,010
I-C3	0,009	0,008	0,009	0,010	-	-	0,014	0,012	0,013	0,011
I-C4	0,012	0,012	0,013	0,013	-	0,012	0,011	0,010	0,010	0,011

Table 5. Average and maximum penetration lengths of the TP07 specimen's features. The features are named as follows: 'C' stands for the step-cylinders from top to bottom.

Feature	Average penetration length, mm										Maximum penetration length, mm									
	0	10	20	30	40	50	60	70	80	90	0	10	20	30	40	50	60	70	80	90
C1	22	23	24	26	30	37	46	51	52	54	41	46	52	66	95	124	124	124	124	125
C2	40	42	44	47	53	58	61	63	64	65	55	68	82	101	114	124	124	124	124	125
C3	56	58	61	64	66	67	67	67	67	67	76	89	106	114	114	124	124	124	124	125
C4	79	77	77	75	73	71	70	69	68	68	107	111	114	114	115	124	124	124	124	125
C5	72	72	65	61	58	56	55	54	53	53	118	119	119	119	119	124	124	124	124	125

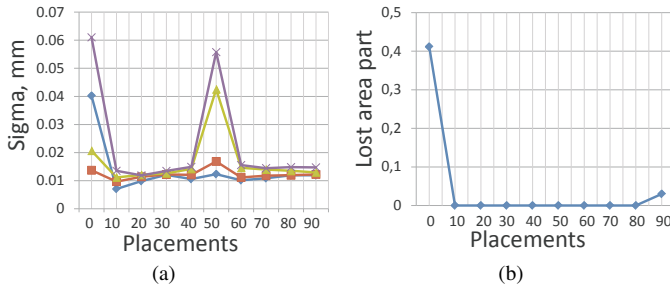


Fig. 15. The plots of the sigma values of the linear distance features (a) and the percentage of the lost surface area (b) for the step-cylinder specimen.

The sigma values of the linear distance features and the percentage of the lost surface area for the step-cylinder are given in Figure 15. And α of 0 degree has the highest lost surface percentage and high sigma values. The high sigma values at 50 degree cannot be explained by the simulation data and are considered to be outliers due to irregularities in the measurement. A unstable positioning of the specimen could be a reason for high sigma values at this placement. For example, if the specimen is slightly tilted during the scanning, this results in blurring and low measurement accuracy. As the neighboring placements have lower sigma values we assume that this placement is an outlier.

The optimal placements for most of the features of both test specimens are predicted by the average and the maximum penetration lengths. For both test specimens the maximum penetration length predicts more optimal placements than the average penetration length. The evaluation shows that prediction can be improved by combining these two parameters. To solve this task the penetration-length distribution of the placement might be used.

9 CONCLUSION

We have presented a tool for visual optimality and stability analysis of 3DCT scan placements. We use a novel 3DCT simulation approach including penetration-length calculation, Radon-space analysis and placement-stability analysis using the stability widget. The tool can be used for determining the optimal specimen placement based on a given geometrical model. Additionally, the tool enables the domain experts to study the correspondence of the penetration lengths and the Radon-space representation of the specimen concerning artifacts and the measurement accuracy. We use programmable GPUs and task parallelization to achieve a better performance. The applicability of the obtained results has been discussed using two real-world specimens.

Our approach has several limitations. One disadvantage is that we do not consider the position of the specimen on the rotary plate. Picking a good position will also affect the outcome. Adding the position of the specimen to the simulation strongly increases the computation time and complicates the visualization and the analysis of the results. In our future work we intend to determine the optimal orientation and the optimal position in sequence. Another limitation of our approach is that it requires a certain number of user interactions. Our system cannot propose the optimal placement fully automatically based on the collected parameters. Furthermore, in our future work we intend to develop a parameter that combines average penetration length, maximum penetration length and percentage of lost surface area. This should increase the accuracy of determining optimal placements.

ACKNOWLEDGMENTS

The presented work has been funded by the Bridge-Project SmartCT and the K-Project ZPT (<http://www.3dct.at>) of the Austrian Research Promotion Agency (FFG). Thanks to the vis-group of the Vienna University of Technology, Institute of Computer Graphics and Algorithms, for support in designing this method and the CT group of the Upper Austrian University of Applied Sciences -Wels Campus for CT measurements, reference measurements and illustrations.

REFERENCES

- [1] J. F. Barrett and K. Nicholas. Artifacts in CT: Recognition and avoidance. *Radiographics* ISSN 0271-5333, vol. 24(6):1679–91, 11 2004.

- [2] U. D. Bordoloi and H.-W. Shen. View Selection for Volume Rendering. *Visualization Conference, IEEE*, 2005.
- [3] L. A. Feldkamp, L. C. Davis, and J. W. Kress. Practical cone-beam algorithm. *J. Opt. Soc. Am. A*, 1(6):612–619, June 1984.
- [4] N. Freud, J.-M. Létang, and D. Babot. *A hybrid approach to simulate multiple photon scattering in X-ray imaging*. *Nuclear Instruments and Methods in Physics Research*. Elsevier, Amsterdam, PAYS-BAS (1984) (Revue), 2005.
- [5] C. Heinzl. *Analysis and Visualization of Industrial CT Data*. PhD thesis, Institute of Computer Graphics and Algorithms, Vienna University of Technology, Favoritenstrasse 9-11/186, A-1040 Vienna, Austria, 12 2009.
- [6] J. Hsieh. *Computed Tomography: Principles, Design, Artifacts and Recent Advances*. SPIE Press, 2 2003.
- [7] G.-R. Jaenisch, C. Bellon, U. Samadurau, M. Zhukovskiy, and S. Podoliako. A Monte Carlo Model Coupled to CAD for Radiation Techniques. *European Conference for NDT 2006*, 2006.
- [8] S. Kasperl. *Qualitätsverbesserungen durch referenzfreie Artefaktreduzierung und Oberflächennormierung in der industriellen 3D-Computertomographie*. PhD thesis, Technische Fakultät der Universität Erlangen Nürnberg, 2005.
- [9] M. M. Malik, C. Heinzl, and M. E. Gröller. Comparative Visualization for Parameter Studies of Dataset Series. *IEEE Transactions on Visualization and Computer Graphics*, 99, 2010.
- [10] M. Mantler, B. Chyba, and M. Reiter. McRay - A Monte Carlo Simulation of Projections in Computed Tomography. *Denver X-ray Conference 2007, Denver (US)*, 7-8 2007.
- [11] K. Mühler, M. Neugebauer, C. Tietjen, and B. Preim. Viewpoint Selection for Intervention Planning. In K. Museth, T. Möller, and A. Ynnerman, editors, *EuroVis*, pages 267–274. Eurographics Association, 2007.
- [12] NVIDIA. *CUDA Programming Guide 2.3*, 2009.
- [13] S. Owada, F. Nielsen, and T. Igarashi. Volume catcher. In *I3D '05: Proceedings of the 2005 symposium on Interactive 3D graphics and games*, pages 111–116, New York, NY, USA, 2005. ACM.
- [14] S. Popov, J. Günther, H.-P. Seidel, and P. Slusallek. Stackless kd-tree traversal for high performance GPU ray tracing. *Computer Graphics Forum*, 26(3):415–424, Sept. 2007. (Proceedings of Eurographics).
- [15] J. Radon. *Über die Bestimmung von Funktionen durch Ihre Integralwerte laengs gewisser Mannigfaltigkeiten*. Berichte über die Verhandlungen der Sächsische Akademie der Wissenschaften, 1917.
- [16] M. Reiter, M. M. Malik, C. Heinzl, D. Salaberger, M. E. Gröller, H. Lettenbauer, and J. Kastner. Improvement of X-Ray image acquisition using a GPU based 3DCT simulation tool. In *International Conference on Quality Control by Artificial Vision*, 5 2009. not peer reviewed, will appear.
- [17] W. Schroeder, K. Martin, and B. Lorensen. *The Visualization Toolkit, Third Edition*. Kitware Inc., 2007.
- [18] B. D. Smith. Image reconstruction from cone-beam projections: necessary and sufficient conditions and reconstruction methods. *IEEE Trans Med Imaging*, 4(1):14–25, 1985.
- [19] J. Tabary, R. Guillemaud, F. Mathy, A. Glière, and P. Hugonnard. Combination of high resolution analytically computed uncollided flux images with low resolution Monte-Carlo computed scattered flux images. *Proc. IEEE-MIC, Norfolk*, pages 551–558, 11 2002.
- [20] S. Takahashi and Y. Takeshima. A Feature-Driven Approach to Locating Optimal Viewpoints for Volume Visualization. In *IEEE Visualization*, pages 495–502. IEEE Press, 2005.
- [21] M. Tory and C. Swindells. Comparing ExoVis, Orientation Icon, and In-Place 3D Visualization Techniques. In *Graphics Interface 03*, pages 57–64, 2003.
- [22] H. K. Tuy. An Inversion Formula for Cone-Beam Reconstruction. *SIAM Journal on Applied Mathematics*, 43(3):546–552, 1983.
- [23] P.-P. Vázquez, M. Feixas, M. Sbert, and W. Heidrich. Viewpoint Selection using Viewpoint Entropy. In *VMV '01: Proceedings of the Vision Modeling and Visualization Conference 2001*, pages 273–280, 2001.
- [24] I. Viola, M. Feixas, M. Sbert, and M. E. Gröller. Importance-Driven Focus of Attention. *IEEE Transactions on Visualization and Computer Graphics*, 12(5):933–940, Oct. 2006.
- [25] L. Zhu, J. Starman, and R. Fahrig. An Efficient Estimation Method for Reducing the Axial Intensity Drop in Circular Cone-Beam CT. *International Journal of Biomedical Imaging*, vol. 2008, 8 2008.